Journal of Materials and Electronic Devices 5 (2024) 22-28

Photoelectric and Diode Characteristics of Al(CdO:ZnO:NiO:Ti)p-Si/Al Schottky Diodes

Erdal KARAKUŞ[1], Çiğdem Şükriye GÜÇLÜ[2], Mümin Mehmet KOÇ[1,3], Burhan COŞKUN[1*]

[1]Kırklareli University, Faculty of Art and Science, Department of Physics, Kırklareli, Türkiye
[2]Gazi University, Faculty of Sciences, Department of Physics, Ankara, Türkiye
[3]Kırklareli University, School of Medical Service, Kırklareli, Türkiye

Solutions containing CdO:ZnO:NiO:Ti composite compounds were produced using sol gel method. CdO:ZnO:NiO:Ti composite solutions were drop cast and spin coated on p-type Si wafer and Al(CdO:ZnO:NiO:Ti)p-SiAl thin films were obtained. Certain photovoltaic characteristics such as photodiode's sensitivity (S:photosensitivity), responsivity (R: photoresponsivity), and specific detectivity (D*: photodetectivity) were derived using various methods. Values for S, R, and D* at an illumination intensity of 100 mW/cm² were found to be 140, 0.024 mW/cm², and 7.2 × 10⁹ Jones, respectively. Fundamental electrical parameters of the Al/(CdO:ZnO:NiO:Ti)/p-Si/Al diode, such as: donor atom concentration (N_A), Fermi energy (E_F), diffusion potential (V_D = Vo + kT/q), depletion region width (W_D), maximum electric field at the junction (E_m), barrier height (Φ_B(C-V)) were assessed. The values of N_A, E_F, $V_D = V_0 + kT/q$, W_D, and Φ_B(C-V) for the fabricated Al/(CdO:ZnO:NiO:Ti)/p-Si/Al diode were obtained from the 1/C² - V graph at 500 kHz as 6.94 × 10¹⁵ cm⁻³, 0.231 eV, 0.79 eV, 3.62 × 10⁻⁵ cm, and 1.16 eV, respectively.

Keywords: *Quaternary Photodiodes; Al/(CdO:ZnO:NiO:Ti)/p-Si/Al; Capacitanca; CdO; Photoelectric Property*

Submission Date: 05 November 2024
Acceptance Date: 28 December 2024

**Corresponding author: burhan.coskun@klu.edu.tr*

1. Introduction

Thin films are essential for modern research and technology thanks to their remarkable physical, chemical, and mechanical capabilities [1,2]. Nanoscale materials are crucial for the advancement of multiple fields, such as optoelectronics, energy storage, sensing technologies, and biological applications [1,2]. The capability to fabricate thin films with customized compositions, thicknesses, and microstructures has facilitated their extensive use in both fundamental research and industrial applications [1,2]. The adaptability of thin films arises from their distinctive characteristics, including a high surface-to-volume ratio, optical transparency, electrical conductivity, and mechanical flexibility [3,4]. These attributes make them suitable candidate for the use in photovoltaics, transistors, light-emitting diodes (LEDs), and protective coatings [5–7]. Thin films are employed in sensors, capacitors, and memory devices, where meticulous regulation of their electrical and optical characteristics is essential [8–10]. Thin films can be classified into three major categories: organic, inorganic, and hybrid thin films [11–13]. Organic thin films consist of carbon-based materials such as organic molecules, carbon nanotubes, graphene, graphite, diamond like carbon. Such materials provide lightweight and flexibility for configurations [14]. They are extensively utilized in organic light-emitting diodes (OLEDs) and organic solar cells because of their economical production and mechanical applicability [15]. Conversely, inorganic thin films demonstrate enhanced thermal stability, elevated

mechanical strength, and exceptional electrical characteristics [3]. Metal oxides and nitrides predominate in this group and are frequently used in semiconductors, photovoltaics, and sensors [16,17]. Hybrid thin films combine the benefits of organic and inorganic materials, offering improved functionality and adjustable features for advanced technologies, such as perovskite solar cells and bioelectronics [18–20].

Metallic thin films are significant due to their superior electrical and thermal conductivity, resistance to corrosion, and catalytic properties. These films are essential for applications in microelectronics, reflective coatings, and energy conversion systems [21,22]. Gold and silver thin films are extensively employed in plasmonic devices, whereas copper and aluminum films function as interconnects in integrated circuits [23,24]. Moreover, metallic films are utilized in sensors, catalysts, and electromagnetic shielding materials, illustrating their versatility and multifunctionality.

ZnO, Cd, Ti, and Ni thin films are especially remarkable for their unique characteristics and prospective applications. For example, Zinc oxide (ZnO) is a transparent semiconductor characterized by a broad bandgap (~3.37 eV), elevated exciton binding energy, and superior optoelectronic characteristics. It is frequently utilized in gas sensors, transparent conductive electrodes, and piezoelectric devices [19,25]. ZnO thin films have biocompatibility, rendering them appropriate for biomedical applications. Cadmium (Cd) thin films, especially cadmium oxide (CdO), demonstrate elevated electrical conductivity and optical transparency, facilitating their application in optoelectronic devices, solar cells, and infrared detectors [26,27]. Cadmium-based films are employed in photo detectors owing to their adjustable bandgap characteristics [28,29]. Titanium (Ti) thin films are distinguished by their remarkable corrosion resistance, elevated strength-to-weight ratio, and biocompatibility [30,31]. These films are extensively utilized in aircraft, biomedical implants, and protective coatings. Moreover, TiO_2 coatings exhibit photocatalytic properties, rendering them appropriate for water purification and self-cleaning surfaces. Nickel (Ni) thin films exhibit superior mechanical strength, magnetic characteristics, and chemical stability, rendering them suitable for use in magnetic storage devices, batteries, and catalysts. Nickel-based films are utilized in anti-corrosion coatings and electromagnetic shielding materials [32–35]. Quaternary functional thin films, consisting of many constituents, provide improved material properties by integrating the distinct attributes of each constituent. These films demonstrate exceptional electrical, optical, and catalytic capabilities, rendering them highly sought after for multifunctional applications [36]. Quaternary thin films are employed in photovoltaic devices, photodetectors, and energy storage systems. Their capacity to offer adjustable bandgaps, superior charge transfer, and increased chemical stability renders them exceptionally versatile for new technologies. Among quaternary thin films, CdO:ZnO:NiO:Ti films have attracted considerable interest due to their diverse characteristics and extensive application possibilities. The combination of CdO and ZnO provides superior optical transparency and conductivity, whereas NiO and Ti enhance structural stability, corrosion resistance, and catalytic efficacy [36]. These films have exceptional photoelectric performance, rendering them suitable candidates for photodiodes, solar cells, and sensors. CdO:ZnO:NiO:Ti thin films demonstrate elevated sensitivity, responsivity, and detectivity, essential for photodetector applications. Their capacity to function efficiently under varying light intensities highlights their appropriateness for optoelectronic devices. Moreover, the structural and electrical characteristics of these films can be meticulously adjusted via compositional engineering, facilitating their application in flexible electronics, transparent conductive coatings, and energy conversion systems.

In this work, we produce CdO:ZnO:NiO:Ti thin films and manufacture Al/(CdO:ZnO:NiO:Ti)/p-Si/Al Schottky diodes. Photovoltaic and capacitance characteristics of the Al/(CdO:ZnO:NiO:Ti)/p-Si/Al derived using various methods.

2. Experimental

The Al/(CdO:ZnO:NiO:Ti)/p-Si/Al Schottky structures were developed on a 300 μm thick p-Si wafer, characterized as <100> float-zone material with a resistivity ranging from 1 to 10 cm-Ω, and polished on one side. Prior to the fabrication, the p-Si wafer underwent a thorough cleaning process [37]. This involved subjecting the p-type silicon wafers to sonication in deionized water for 5 minutes, followed by another 5 minutes of sonication in ethanol, and concluding with a final 5-minute sonication in deionized water. A solution of hydrofluoric acid (HF) diluted in water at a ratio of 1:10 ml was prepared, sonicated for 5 minutes, and subsequently rinsed with pure water. The samples were then dried using nitrogen gas. Wafers measuring 2 cm x 2 cm were cut, and six layers of film were spin-coated onto the substrates. Each layer was applied using a spin-coating process at 3000 rpm for 30 seconds, followed by drying on a hot plate.

Subsequently, the wafer was placed in a vacuum chamber where high-purity gold (99.999%) was thermally evaporated onto the backside of the p-Si wafer to a thickness of 150 nm, utilizing a high-vacuum metal evaporation system operating at a pressure of 10^{-6} Torr. The wafer underwent annealing at 500 °C in a nitrogen atmosphere to achieve low resistivity

and establish good ohmic contact. Following this, the (CdO:ZnO) solution was applied to the front of the p-Si wafer as an interfacial layer via the spin-coating technique. This solution was prepared by dissolving zinc acetate ($Zn(CH_3COO)_2$) and nickel chloride ($NiCl_2$) in 15 ml of methoxyethanol to create 0.1 M solutions of zinc and nickel, respectively. A 0.4 M base solution was also prepared by dissolving sodium hydroxide (NaOH) in 65 ml of methanol. The synthesis of ZnO and Cd involved agitating the 0.1 M zinc solution and the 0.4 M base solution separately for 10 minutes at 500 rpm, with ethanolamine acting as a stabilizer. The coated films were dried for one hour at 50 °C on a hot plate to form solid films.

For further enhancement, PCBM, a derivative of fullerene, was coated onto the front of the p-Si wafer for 30 seconds at 2000 rpm and 80 °C using a Fytronix spin coater system. The temperature of 80 °C was critical for achieving optimal coating properties, facilitating the formation of a highly homogeneous layer with improved adhesion to the substrate. After the coating, PCBM was dissolved in chlorobenzene. Finally, high-purity aluminium, with a diameter of 1 mm and a thickness of 150 nm, was deposited onto the (Cd:ZnO) interlayer using the same thermal evaporation system. The thickness of both the rectifier Al Schottky contacts and the backside Au ohmic contacts, along with their deposition rates, were monitored using a quartz crystal metal thickness meter.

For electrical measurements, thin silver-coated wires were utilized as the electrode connection system, and the fabricated samples were mounted on a copper holder. Characterization measurements were conducted using the Fytronix-FY-7000 characterization system within a Fytronix cryostat at approximately 10^{-3} Torr to minimize external influences. All device characterization equipment was supplied by Fytronix.

3. Results

3.1 Photoelectric properties of Al/(CdO:ZnO:NiO:Ti)/p-Si/Al diodes

The photoelectric properties of the manufactured Al/(CdO:ZnO:NiO:Ti)/p-Si/Al photodiodes were analyzed under both dark conditions and an illumination intensity of 100 mW/cm². This analysis utilized I_R-V_R data collected under reverse bias at the same illumination intensity. The values for the photodiode's S, R and D* were derived using the equations outlined below. The variations of these parameters with respect to voltage are illustrated in Figures 1, 2, and 3, respectively.

$$S = (I_{ph} - I_{dark})/I_{dark} \quad (1)$$

$$R = (I_{ph} - I_{dark})/P.A \quad (2)$$

$$D^* = R(A / (2qI_{dark}))^{0.5} \quad (3)$$

In these equations, I_{dark} and I_{ph} refer to the current values recorded under dark conditions and varying light illumination intensities, respectively. P signifies the light intensity that is shed on the diode, while A represents the area of the diode. As illustrated in Figures 1, 2, and 3, the values of S, R, and D* show a considerable dependence on the voltage applied. Specifically, the peak values for S, R, and D* at an illumination intensity of 100 mW/cm² were found to be 140, 0.024 mW/cm², and 7.2 × 10⁹ Jones, respectively. These findings indicate that the Al/(CdO:ZnO:NiO:Ti)/p-Si/Al diode exhibits a high sensitivity to the light, making the diodes a suitable candidate for use in optoelectronic applications such as photodiodes, solar cells, and photodetectors [38–42] .

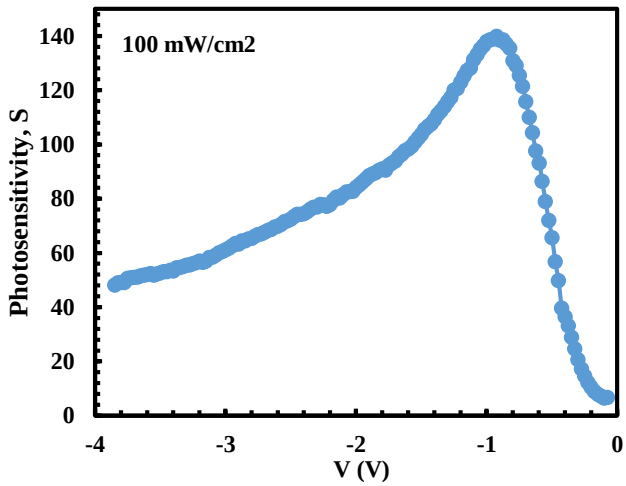

Figure 1: S-V graph of Al/(CdO:ZnO:NiO:Ti)/p-Si/Al diode obtained under 100mW/cm² illumination

3.2 Capacitance properties of Al/(CdO:ZnO:NiO:Ti)/p-Si/Al diodes

The diode parameters derived from forward bias I-V measurements are distinct from those obtained by forward bias C-V measurements. This is since, under reverse bias, the barrier faced by electrons transitioning from the semiconductor to the metal is approximately equivalent to the Fermi energy (E_F), which exceeds the barrier encountered by electrons traveling from the metal to the semiconductor. Consequently, only the capacitance-voltage measurements of the constructed photodiodes in darkness were performed utilizing an HP-4192A LF impedance analyzer at 500 kHz, within a voltage range of ±2.5V in 50 mV increments, as illustrated in Figure 4.

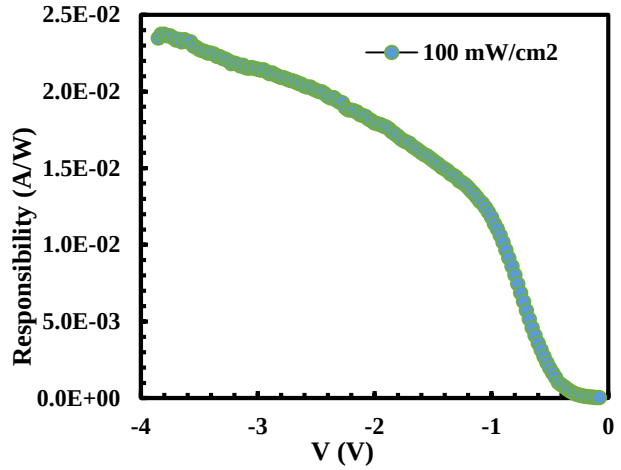

Figure 2: R-V graph of Al/(CdO:ZnO:NiO:Ti)/p-Si/Al diode obtained under 100mW/cm^2 illumination

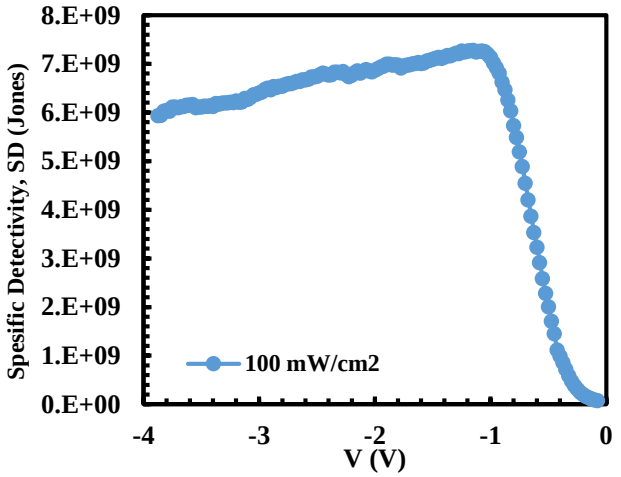

Figure 3: D*-V graph of Al/(CdO:ZnO:NiO:Ti)/p-Si/Al diode obtained under 100mW/cm^2 illumination

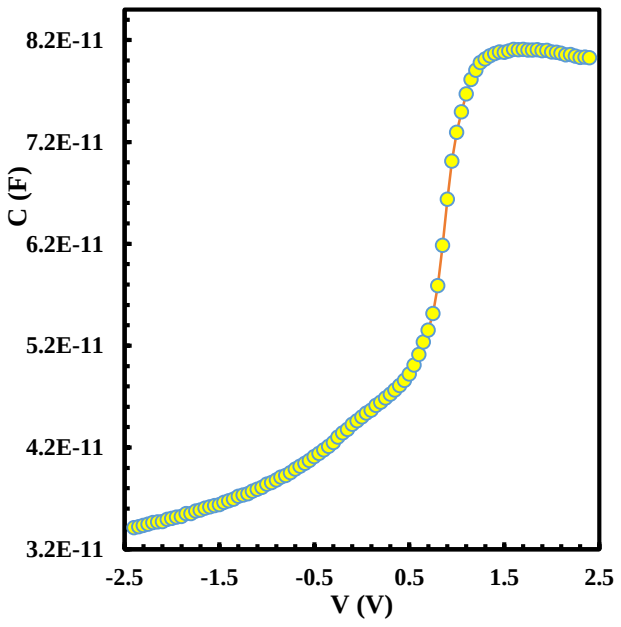

Figure 4: C-V graph of Al/(CdO:ZnO:NiO:Ti)/p-Si/Al diode obtained at 500 kHz.

The C-V curves demonstrate three separate behaviors: accumulation (about 1.2 to 2.5V), depletion (from -1V to +1.2V), and inversion (around -2.5 to -1V). These actions are analogous to those of a metal/oxide/semiconductor (MOS) capacitor, which is an anticipated trait. This phenomenon transpires as soon as contact is made between the metal and the semiconductor, prompting the majority carriers (holes) in the p-Si to migrate towards the metal's front surface. Consequently, the C (=Q/V) value begins to diminish. Consequently, because of such a diffusion process, the front surface of the p-Si semiconductor acquires a negative charge, whilst the front surface of the metal attains a positive charge, leading to an inversion of their starting states.

The depletion-region capacitance (*C*) of a MIS-type diode is defined as follows [43–45]:

$$C = \frac{|\partial Q_{SC}|}{\partial V} = \sqrt{\frac{q\varepsilon_s\varepsilon_0 N_A}{2\left(V_D - V - \frac{kT}{q}\right)}} \quad (4)$$

where ε_s and ε_0 are the dielectric constants of the semiconductor and free space, respectively; A is the area of the Schottky contact, V_R is the reverse bias voltage applied to the diode, and V_d is obtained from the intersection point of the voltage axis in the C^{-2}-V graph, where the C^{-2} axis (y-axis) equals zero ($V_D = V_o + kT/q$). Using this information, other fundamental electrical parameters of the Al/(CdO:ZnO:NiO:Ti)/p-Si/Al diode, such as:

- Donor atom concentration (N_A)
- Fermi energy (E_F)
- Diffusion potential ($V_D = Vo + kT/q$)
- Depletion region width (W_D)
- Maximum electric field at the junction (E_m)
- Barrier height (Φ_B(C-V))

were calculated using the equations provided below, based on the intercept and slope of the reverse bias linear C^{-2}-V curve presented in Figure 5.

$$C^{-2} = \frac{2(V_R + V_o)}{q\varepsilon_s\varepsilon_o A^2 N_D} \quad (5)$$

$$E_F = \frac{kT}{q} ln\left(\frac{N_C}{N_D}\right) \quad (6)$$

$$W_D = \left(\frac{2\varepsilon_s\varepsilon_o V_D}{qN_D}\right)^{1/2} \quad (7)$$

$$E_m = \left(\frac{2qN_D V_o}{\varepsilon_s\varepsilon_o}\right)^{1/2} \quad (8)$$

$$\Delta\Phi_B = (\frac{2E_m}{4\pi\varepsilon_o})^{1/2} \quad (9)$$

Thus, the potential energy barrier formed between the metal and the semiconductor was obtained using the following equation, based on the calculated V_o and E_F values.

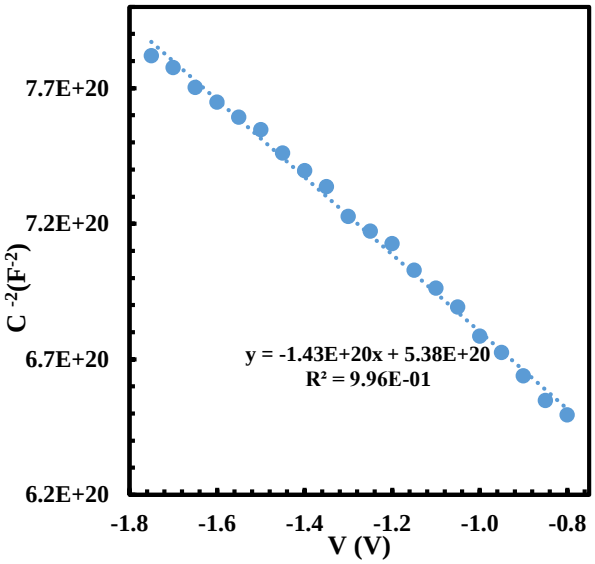

Figure 5: C^{-2} - V graph of Al/(CdO:ZnO:NiO:Ti)/p-Si/Al diode obtained at 500 kHz under reverse bias.

$$\Phi_B = V_0 + \frac{kT}{q} + E_F \quad (10)$$

The values of N_A, E_F, $V_D = V_o + kT/q$, W_D, and Φ_B(C-V) for the fabricated Al/(CdO:ZnO:NiO:Ti)/p-Si/Al diode were obtained from the $1/C^2$ - V graph at 500 kHz as 6.94×10^{15} cm^{-3}, 0.231 eV, 0.79 eV, 3.62×10^{-5} cm, and 1.16 eV, respectively.

The Φ_B(C-V) = 1.16 eV value obtained from the reverse bias $1/C^2$ - V graph is higher than the value obtained from the forward bias Ln(I)-V graph. This discrepancy arises from the nature of the measurement and calculation methods used.

Recently, similar studies have been conducted in the literature, and comparable characteristics have been observed [36,40,46].

4. Conclusion

In the study, we produce CdO:ZnO:NiO:Ti thin films and manufacture Al(CdO:ZnO:NiO:Ti)p-Si/Al Schottky diodes. Photovoltaic and capacitance characteristics of the Al(CdO:ZnO:NiO:Ti)p-Si/Al derived using various methods. The values for the photodiode's sensitivity, response, and specific detectivity were derived. Values for S, R, and D* at an illumination intensity of 100 mW/cm² were found to be 140, 0.024 mW/cm², and 7.2×10^9 Jones, respectively. The values of N_A, E_F, $V_D = V_o + kT/q$, W_D, and Φ_B(C-V) for the fabricated Al/(CdO:ZnO:NiO:Ti)/p-Si/Al diode were obtained from the $1/C^2$ - V graph at 500 kHz as 6.94×10^{15} cm^{-3}, 0.231 eV, 0.79 eV, 3.62×10^{-5} cm, and 1.16 eV, respectively.

References

[1] Kaya E, Coşkun B (2023) An Overview for Fundamental Chemical Characterization Techniques for Thin Films and Nanostructures. Journal of Materials and Electronic Devices 2 33–38. https://www.dergi-fytronix.com/index.php/jmed/article/view/266

[2] Frey H (2015) Applications and Developments of Thin Film Technology, in: Handbook of Thin-Film Technology. Springer Berlin Heidelberg, Berlin, Heidelberg, pp. 1–3. https://doi.org/10.1007/978-3-642-05430-3_1

[3] Alexopoulos PS, O'Sullivan TC (2003) Mechanical Properties of Thin Films. Annual Review of Materials Science 20 391–420. https://doi.org/10.1146/ANNUREV.MS.20.080190.002135

[4] Wang X, Liao Y, Zhang D, Wen T, Zhong Z (2018) A review of Fe_3O_4 thin films: Synthesis, modification and applications. J Mater Sci Tech 34 1259–1272. https://doi.org/10.1016/J.JMST.2018.01.011

[5] Han K, Yoon S, Chung WJ (2015) CdS and CdSe Quantum Dot-Embedded Silicate Glasses for LED Color Converter. Int J Appl Glass Sci 6 103–108. https://doi.org/10.1111/ijag.12115

[6] Baek SM, Shirafuji T, Saito N, Takai O (2011) Fabrication of transparent protective diamond-like carbon films on polymer. Jpn J Appl Phys 50 https://doi.org/10.1143/JJAP.50.08JD08

[7] Güngör ZG, Coşkun B, İlhan M, Koç MM (2023) Photovoltaic investigation of Al/p-Si/CuPc/Al Photodiodes. Kirklareli University Journal of Engineering and Science 9 36–47. https://doi.org/10.34186/KLUJES.1288961

[8] Wang Y, Song Y, Xia Y (2016) Electrochemical capacitors: Mechanism, materials, systems, characterization and applications. Chem Soc Rev 45 5925–5950. https://doi.org/10.1039/c5cs00580a

[9] Dere A, Yakuphanoglu F (2021) Polyvinylidene fluoride shape memory polymer for dielectric

device applications. Journal of Materials and Electronic Devices 5 28–32. https://dergi-fytronix.com/index.php/jmed/article/view/180

[10] Yamazoe N, Sakai G, Shimanoe K (2003) Oxide semiconductor gas sensors. Catalysis Surveys from Asia 7 63–75. https://doi.org/10.1023/A:1023436725457

[11] Aslan N, Aksakal B, Dikici B, Sinirlioglu ZA (2022) Graphene reinforced hybrid-bioceramic coatings on porous-Ti6Al4V for biomedical applications: morphology, corrosion resistance, and cell viability J Mater Sci 57 16858–16874. https://doi.org/10.1007/S10853-022-07695-7

[12] Wang FM, Chen MW, Lai QB (2010) Metallic contacts to nitrogen and boron doped diamond-like carbon films. Thin Solid Films 518 3332–3336. https://doi.org/10.1016/J.TSF.2009.10.041

[13] Oruç Ç, Erkol A, Altındal A (2016) Conduction Mechanisms in Organic-based Rectifying Diode. Anadolu University Journal of Science and Technology A - Applied Sciences and Engineering 17 717–723. https://doi.org/10.18038/AUBTDA.267118

[14] Ling H, Liu S, Zheng Z, Yan F, Ling HF, Liu SH, Yan F, Zheng ZJ (2018) Organic Flexible Electronics Small Methods 2 1800070. https://doi.org/10.1002/SMTD.201800070

[15] Ho CL, Li H, Wong WY (2014) Red to near-infrared organometallic phosphorescent dyes for OLED applications. J Organomet Chem 751 261–285. https://doi.org/10.1016/J.JORGANCHEM.2013.09.035

[16] Mekki A, Ocaya RO, Dere A, Al-Ghamdi AA, Harrabi K, Yakuphanoglu F (2016) New photodiodes-based graphene-organic semiconductor hybrid materials. Synth Met 213 47–56. https://doi.org/10.1016/j.synthmet.2015.12.026

[17] Karabulut A, Dere A, Al-Sehemi AG, Al-Ghamdi AA, Yakuphanoglu F (2018) Cadmium Oxide:Titanium Dioxide Composite Based Photosensitive Diode. Journal of Electronic Materials 2018 47:12 47 7159–7169. https://doi.org/10.1007/S11664-018-6647-1

[18] Aslan F, Esen H, Yakuphanoğlu F (2019) Electrical and fotoconducting characterization of Al/coumarin:ZnO/Al novel organic-inorganic hybrid photodiodes. J Alloys Compd 789 595–606. https://doi.org/10.1016/j.jallcom.2019.03.090

[19] Kurt MS, Aktaş S, Ünal F, Kabaer M (2022) Optical and Electrical Characterization of a ZnO/Coronene-Based Hybrid Heterojunction Photodiode. J Electron Mater 1–12. https://doi.org/10.1007/S11664-022-09910-2

[20] Xiao Y, Han G, Chang Y, Zhou H, Li M, Li Y (2014) An all-solid-state perovskite-sensitized solar cell based on the dual function polyaniline as the sensitizer and p-type hole-transporting material. J Power Sources 267 1–8. https://doi.org/10.1016/j.jpowsour.2014.05.053

[21] Zambrano DF, Villarroel R, Espinoza-González R, Carvajal N, Rosenkranz A, Montaño-Figueroa AG, Arellano-Jiménez MJ, Quevedo-Lopez M, Valenzuela P, Gacitúa W (2021) Mechanical and microstructural properties of broadband anti-reflective TiO_2/SiO_2 coatings for photovoltaic applications fabricated by magnetron sputtering. Solar Energy Materials and Solar Cells 220 110841. https://doi.org/10.1016/J.SOLMAT.2020.110841

[22] Wang Y, Wei W, Li F, Huang B, Dai Y (2020) Janus Bi_2XYZ monolayers for light harvesting and energy conversion from first-principles calculations. Physica E Low Dimens Syst Nanostruct 117 113823. https://doi.org/10.1016/j.physe.2019.113823

[23] Yakubovsky DI, Arsenin AV, Stebunov YV, Fedyanin DY, Volkov VS (2017) Optical constants and structural properties of thin gold films. Optics Express, Vol. 25, Issue 21, Pp. 25574-25587 25 25574–25587. https://doi.org/10.1364/OE.25.025574

[24] Gezgin SY, Kılıç HŞ, Kepceoğlu A, Bayır S, Nalbantoğlu IE, Toprak A (2016) Plasmonic tuning of gold doped thin films for layers of photovoltaic devices. AIP Conf Proc 1722. https://doi.org/10.1063/1.4944228/648779

[25] Çağlar M, Yakuphanoğlu F (2012) Structural and optical properties of copper doped ZnO films derived by sol-gel. Appl Surf Sci 258 3039–3044. https://doi.org/10.1016/j.apsusc.2011.11.033

[26] Özden S, Koç MM (2018) Spectroscopic and microscopic investigation of MBE-grown CdTe (211) B epitaxial thin films on GaAs (211) B substrates. Appl Nanosci 8 891–903. https://doi.org/10.1007/s13204-018-0727-7

[27] İlhan M, Görünmez Güngör Z, Koç MM, Coşkun B, Yakuphanoğlu F (2023) Infrared light sensing performance of CdO-doped TiO_2 thin films. Journal of Materials Science: Materials in Electronics 34 1–11 https://doi.org/10.1007/S10854-022-09411-2

[28] Coşkun B (2019) Capacitance and Dielectric Properties of Mn Doped CdO Photodetectors. Journal of Materials and Electronic Devices 1 65–71.

[29] Dugan S, Koç MM, Coşkun B (2019) Structural, electrical and optical characterization of Mn doped CdO photodiodes. J Mol Struct 1205 127235. https://doi.org/10.1016/J.MOLSTRUC.2019.127235

[30] Aslan N, Koç MM, Dere A, Arif B, Erkovan M, Al-Sehemi AG, Al-Ghamdi AA, Yakuphanoğlu F (2018) Ti doped amorphous carbon (Al/Ti-a:C/p-Si/Al) photodiodes for optoelectronic applications. J Mol Struct 1155 813–818. https://doi.org/10.1016/j.molstruc.2017.11.050

[31] Saha B, Thapa R, Chattopadhyay KK (2008) Bandgap widening in highly conducting CdO thin film by Ti incorporation through radio frequency magnetron sputtering technique. Solid State Commun 145 33–37. https://doi.org/10.1016/J.SSC.2007.10.001

[32] Erkovan M, Shokr YA, Schiestl D, Wu CB, Kuch W(2015) Influence of NixMn1−x thickness and composition on the Curie temperature of Ni in NixMn1−x/Ni bilayers on Cu3Au(001). J Magn Magn Mater 373 151–154. https://doi.org/10.1016/J.JMMM.2014.02.017

[33] Kurnaz Yetim N, Aslan N, Sarıoğlu A, Sarı N, Koç MM (2020) Structural, electrochemical and optical properties of hydrothermally synthesized transition metal oxide (Co_3O_4, NiO, CuO) nanoflowers. Journal of Materials Science: Materials in Electronics 31 12238–12248. https://doi.org/10.1007/s10854-020-03769-x

[34] Kurnaz Yetim N (2020) Hidrotermal olarak Sentezlenen Çiçek benzeri NiO@Fe_3O_4'ün Katalitik Özellikleri. Düzce Üniversitesi Bilim ve Teknoloji Dergisi 8 1964–1974. https://doi.org/10.29130/dubited.721970

[35] Bai G, Dai H, Deng J, Liu Y, Ji K (2012) Porous NiO nanoflowers and nanourchins: Highly active catalysts for toluene combustion. Catal Commun 27 148–153. https://doi.org/10.1016/j.catcom.2012.07.008

[36] Altındal Yerişkin S, Dere A, Orman Y, Yakuphanoğlu F (2024), Quaternary functional semiconductor devices. Phys Scr 99 (2024) 075958. https://doi.org/10.1088/1402-4896/AD4F30

[37] Özden S, Koç MM (2019) Wet-chemical etching of GaAs (211) B wafers for controlling the surface properties. International Journal of Surface Science and Engineering 13 79. https://doi.org/10.1504/IJSURFSE.2019.102359

[38] Alptekin S, Altındal Ş (2020) Electrical characteristics of Au/PVP/n-Si structures using admittance measurements between 1 and 500 kHz. Journal of Materials Science: Materials in Electronics 31 (2020) 13337–13343. https://doi.org/10.1007/S10854-020-03887-6

[39] Cheung SK, Cheung NW (1986) Extraction of Schottky diode parameters from forward current-voltage characteristics. Appl Phys Lett 49 85–87. https://doi.org/10.1063/1.97359

[40] Al-Sehemi AG, Karabulut A, Dere A, Al-Ghamdi AA, Yakuphanoğlu F (2022) Photodiode performance and infrared light sensing capabilities of quaternary Cu_2ZnSnS_4 chalcogenide. Surfaces and Interfaces 29 101802. https://doi.org/10.1016/J.SURFIN.2022.101802

[41] Lapa HE, Kökce A, Aldemir DA, Özdemir AF (2021) The response of high barrier Schottky diodes to light illumination. Journal of Materials Science: Materials in Electronics 32 4448–4456. https://doi.org/10.1007/S10854-020-05186-6.

[42] Ganj T, Rozati SM, Azizian-Kalandaragh Y, Pirgholi-Givi G, Altındal Ş (2023) The effect of (CeO_2: PVC) thin interfacial film on the electrical features in Au/n-Si Schottky barrier diodes (SBDs) by using current–voltage measurements. Journal of Materials Science: Materials in Electronics 34 1–13. https://doi.org/10.1007/S10854-023-10094-6.

[43] Sze SM, Li Y, Kwok K Ng (2021) Physics of semiconductor devices. John Wiley & Sons, Inc., Hsinchu.

[44] Tung RT (2001) Recent advances in Schottky barrier concepts. Materials Science and Engineering: R: Reports 35 1–138. https://doi.org/10.1016/S0927-796X(01)00037-7

[45] Sharma B (1984) Metal-Semiconductor Schottky Barrier Junctions and Their Applications. Plenum Press, New York.

[46] Radaf IME (2023) Detailed analysis of the electrical and photovoltaic characteristics of Al/$Cu_2ZnGeSe_4$/n-Si/Ag heterojunction. Indian Journal of Physics 97 3827–3833. https://doi.org/10.1007/S12648-023-02708-W